encit 2020

ABCM
Associação Brasileira de Engenharia e Ciências Mecânicas

18th Brazilian Congress of Thermal Sciences and Engineering
November 16–20, 2020 (Online)

ENC-2020-302
Determining the granular temperature of gas fluidized beds in narrow tubes

Karlo Fernandes Rocha[a,b,1]
Fernando David Cúñez Benalcázar[a,2]
Erick de Moraes Franklin[a,3]
[a]University of Campinas, School of Mechanical Engineering, Rua Mendeleyev, 200, Campinas, 13083-860, Brazil
[b]Federal Institute of Espírito Santo, Rodovia BR-482 (Cachoeiro-Alegre), 29300-970, Cachoeiro de Itapemirim, ES, Brazil
[1]karlor@ifes.edu.br, [2]fernandodcb@fem.unicamp.br, [3]franklin@fem.unicamp.br

Abstract. *This work reports a numerical study of granular temperature in gas-solid fluidized beds by using an Eulerian-Lagrangian approach (CFD-DEM). The numerical simulations were performed using the open source codes CFDEM, OpenFOAM and LIGGGHTS. The bed was formed in a vertical tube with a diameter of* $D = 2.5$ *mm which was filled with glass spheres with a diameter of* $d = 0.5$ *mm. The bed consisted of 600 glass beads, and two air flows that correspond to cross-sectional mean velocities of* $\overline{U} = 1.05$ *and* $\overline{U} = 1.15$ *m/s were imposed at the bottom of the tube. The granular temperature was computed by averaging the instantaneous velocities using the concepts of kinetic theory. With these conditions, we observe the formation of alternating high- and low-compactness regions, known as plugs and piston bubbles, and we tracked every single particle and the local volume fraction to obtain the main behavior of the granular temperature in the plugs and bubbles. The values of the granular temperature for the vertical direction,* (z *direction), is an order of magnitude larger than that for the transverse directions,* (x, y *directions). We observed anisotropy of the granular temperature is consistent with the conclusions reported in literature.*

Keywords: *Granular temperature, fluidized bed, gas-solid, plugs, bubbles, CFD-DEM.*

1. INTRODUCTION

Fluidized beds are widely applied in industrial processes for mixing, coating, drying, catalytic and non-catalytic reactions, and many others applications. In the case of gas-solid fluidized beds, when the velocity of the fluid flow is increased to a certain value, the drag force exerted by the fluid balances with the weight of the particles, reaching thus the suspension of particles. This velocity is known as minimum velocity of fluidization. At higher flow rates the bed may become unstable and part of the fluid passes through the bed in the form of bubbles or slugs. Bubbles occur in beds where the diameter of the tube is large when compared to the grain diameter and is characterized by regions of voids that propagate upwards along the bed, whereas plugs and piston bubbles occur in narrow beds and are characterized by compact regions of high and low concentration of particles, respectively (Cúñez and Franklin, 2019, 2020b). Gas-solid fluidized beds in wide tubes are very unstable and rapidly reach a bubbling regime. Several studies investigated the instabilities appearing in gas fluidized beds in large tubes (Tsuji *et al.*, 1992; Hoomans *et al.*, 1996; Zhou *et al.*, 2010; Goldschmidt *et al.*, 2002; Xu *et al.*, 2007; Wu *et al.*, 2013; Kafui *et al.*, 2002). These studies, experimental and numerical have been extensively developed to dense gas-solid fluidized beds in order to obtain the time-averaged solids circulation patterns, bubble size, and velocity distribution.

Researchers have developed a variety of computational fluid dynamics (CFD) models that describe gas-solid flows at different levels of detail. Many numerical studies have investigated the instabilities in the gas-solid system by using an Eulerian-Eulerian numerical approach. In those simulations, the fluid and solid phases are considered as a continuous media and both can be solved by computational fluid dynamics (CFD), this approach being also called Two-Fluid Model (TFM) (Cammarata *et al.*, 2003; Mahinpey *et al.*, 2007; Hosseini *et al.*, 2009). Other studies in the literature have used an Eulerian-Lagrangian approach for the study of fluidized beds (Tsuji *et al.*, 1992; Hoomans *et al.*, 1996; Zhou *et al.*, 2010; Goldschmidt *et al.*, 2002) where the solid phase is considered as discrete medium and the fluid phase is considered as a continuous medium. The solid phase, based on the Discrete Element Method (DEM, (Cundall and Strack, 1979)), is solved by Newton's second law of motion applied to a discrete system, while the fluid phase, based on (CFD), is computed by solving by Navier Stokes equations; this approach is also known as CFD-DEM. Several studies (Tsuji *et al.*, 1992; Hoomans *et al.*, 1996; Zhou *et al.*, 2010) have demonstrated that CFD-DEM simulations can predict the hydrodynamics of large fluidized beds well. In the case of narrow beds, Cúñez and Franklin (2019, 2020b) showed that CFD-DEM simulations reproduce well the formation of granular plugs and the segregation of grains in solid-liquid fluidized beds.

The granular temperature, based on the fluctuation of particle velocity, which consists in the kinetic energy associated with individual particle velocities, is one of the most important parameters to measure the kinetic behavior in particulate

systems. Holland *et al.* (2008) and Müller *et al.* (2008) reported time-averaged measurements of the granular temperature in gas-fluidized beds using a magnetic resonance technique, and found a good agreement with their simulation results. Employing experiments and numerical simulations Tartan and Gidaspow (2004) and Jung *et al.* (2005), proposed two granular temperatures due to different kinds of oscillations of particles. The first one is due to random oscillations of particles and is called as particle granular temperature. The second one, bubble granular temperature, is caused by formations and motions of bubbles. The granular temperature is calculated as a local spatial average per unit of volume, so that, to avoid statistical errors, one chooses volumes where the spatial variations are homogeneous (Tang *et al.*, 2016). Recently, Cúñez and Franklin (2020a) showed variations of the granular temperature during cristallization and jamming occuring in solid-liquid fluidized beds in very narrow tubes. For that, they computed the granular temperature based on the deviations of the instantatous velocity of each grain from the average value of the ensemble of grains.

In this work, we performed CFD-DEM computations to investigate the granular temperature in gas-solid fluidized beds in very narrow tubes, where the formation of alternating high- and low-compactness regions usually appear. The main objective was to investigate the granular temperature in the plug and bubble regions. The gas-solid fluidized beds were formed in a 5 cm long vertical tube with a diameter of $D = 2.5$ mm and consisted of glass spheres with a diameter of $d = 0.5$ mm and density of $\rho_p = 2500$ kg/m^3. Thus, the ratio between the tube and the particles was $D/d = 5$. We report the particle granular temperature based on the spatial averaging of squared fluctuation velocity of particles. This granular temperature corresponds to the first definition proposed by Tartan and Gidaspow (2004); Jung *et al.* (2005).

2. FORMULATION OF THE NUMERICAL MODEL

2.1 Governing equations

The mass and momentum equations for the gas phase are given respectively by:

$$\frac{\partial \rho_f \varepsilon_f}{\partial t} + \nabla \cdot (\rho_f \varepsilon_f \vec{u}_f) = 0 \tag{1}$$

$$\frac{\partial \rho_f \varepsilon_f \vec{u}_f}{\partial t} + \nabla \cdot (\rho_f \varepsilon_f \vec{u}_f \vec{u}_f) = -\varepsilon_f \nabla P + \varepsilon_f \nabla \cdot \vec{\vec{\tau}} + \rho_f \varepsilon_f \vec{g} + \vec{F}_{p,f} \tag{2}$$

where P represent the pressure, $\vec{g}$ is the acceleration of gravity, $\vec{\vec{\tau}}$ is the stress tensor and $\rho_f, \varepsilon_f, \vec{u_f}$ are the density, volume fraction and mean velocity of the fluid, respectively. The last term $\vec{F}_{p,f}$ on the right represents the drag force per volume, is computed by Gidaspow model (Gidaspow, 1994) and given by:

$$\vec{F}_{p,f} = \frac{1}{V_{cell}} \sum \vec{F}_d = \frac{1}{V_{cell}} \sum \frac{V_{p_i} \beta}{(1-\varepsilon_f)} (\vec{u}_f - \vec{u}_p) \tag{3}$$

where β is the coefficient of momentum transfer between phases due to the drag force, V_{cell} is the volume of each cell and V_{p_i} is the volume of particle i in cell. The coefficient β is given by:

$$\beta = \begin{cases} 150 \dfrac{(1-\varepsilon_f)^2 \mu_f}{\varepsilon_f d_p^2} + 1.75 \dfrac{\rho_f |\vec{u}_f - \vec{u}_p| (1-\varepsilon_f)}{d_p}, & \varepsilon_f < 0.8 \\ \dfrac{3}{4} C_d \dfrac{\rho_f \varepsilon_f (1-\varepsilon_f) |\vec{u}_f - \vec{u}_p|}{d_p} \varepsilon_f^{-2.65}, & \varepsilon_f \geq 0.8 \end{cases} \tag{4}$$

where C_d is the drag coefficient and is related to the particle Reynolds number by:

$$C_d = \begin{cases} \dfrac{24}{Re_p} \left(1 + 0.15 \left(Re_p\right)^{0.687}\right), & Re_p < 1000 \\ 0.44, & Re_p \geq 1000 \end{cases} \tag{5}$$

with

$$Re_p = \frac{\rho_f \varepsilon_f d_p |\vec{u}_f - \vec{u}_p|}{\mu_f}. \tag{6}$$

For the solid phase, the motion of each particle is calculated by linear and angular momentum equations and are given by:

$$m_p \frac{d\vec{u}_p}{dt} = -V_p \nabla P + V_p \nabla \cdot \vec{\vec{\tau}} + m_p \vec{g} + \left[\sum_{i,j} \vec{F}_{c,i,j} + \sum_{i,w} \vec{F}_{c,i,w} \right] - V_p \vec{F}_{p,f} \tag{7}$$

$$I_p \frac{d\vec{\omega}}{dt} = \sum_{i,j} \vec{T}_{p,i,j} + \sum_{i,w} \vec{T}_{p,i,w} \tag{8}$$

where $\vec{u_p}$, m_p, V_p are the velocity, mass and volume of solid particles, respectively. T_p is the torque from the tangential component of the contact force, and I_p and $\vec{\omega}$ are the moment of inertia and angular velocity of a particle, respectively.

For particle-particle interactions, the spring-dashpot model is employed for the contact force $\vec{F}_{c,i,j} = \vec{F}_{cn,i,j} + \vec{F}_{ct,i,j}$ where $\vec{F}_{cn,i,j}$ and $\vec{F}_{ct,i,j}$ are normal and tangential components. The main equations of the spring-dashpot model are described in Cundall and Strack (1979).

2.2 Numerical setup

In the numerical simulations, we considered a gas-solid fluidized bed in a 5 cm long vertical tube with a diameter of $D = 2.5$ mm and consisted of glass spheres with a diameter of $d = 0.5$ mm, and the fluid was air. The bed consisted of 600 glass beads, and two air flows that correspond to cross-sectional mean velocities of $\overline{U} = 1.05$ and $\overline{U} = 1.15$ m/s were imposed at the tube inlet. Initially, the particles are randomly inserted to fall freely without air flow until they reach the bottom of the tube. After a certain time, the bed reaches a stable state with velocity of the particles equal to zero. Afterwards, the fluid flow is imposed at the inlet. The side walls of the tube are impenetrable and with non-slip conditions for the fluid. The superficial velocity $\overline{U}$ is imposed as the velocity of the air in the vertical direction at the bottom of the tube, where the velocity gradient of the fluid is set to zero.

This computations are based on Eulerian-Lagrangian method. The fluid flow is solved with CFD with the open source code OpenFOAM (www.openfoam.com), the granular motion is solved with the open source code LIGGGHTS (www.liggghts.com) which is based on DEM, and CFD-DEM coupling is made with the open source code CFDEM (www.cfdem.com). A three dimensional geometry of a vertical tube was created and a hexahedral mesh was generated with a total number of 38.400 cells. We employed a big particle void fraction model (www.cfdem.com), which is used when the particle is larger than the CFD cells. With the generated mesh, the behavior of the grains inside the fluid flow was well captured (Cúñez and Franklin, 2019). For our CFD-DEM simulations, the one-phase air flow is in laminar regime ($Re = O(100)$), so that we considered a laminar regime. In addition, the fluctuations of the particles and the particle-particle interactions are more energetic than the velocity fluctuations of the fluid flow; therefore, an increase in mesh refinement is unnecessary. We ran the numerical simulations over 5 seconds for all the cases. For that, each run took approximately 8 to 10 hours to be completed. Finally, all the simulations were performed using a configuration hardware Intel Core i7-4770 3.40GHz with 4 core and 12 GB RAM.

The numerical parameters used in simulations are: tube diameter $D = 2.5$ mm; number of particles $N = 400$ and $N = 600$; particle diameter $d = 0.5$ mm; particle density $\rho_p = 2500$ Kg/m^3; gas density $\rho_f = 1.2$ Kg/m^3; gas viscosity $\mu_f = 1.8$ kg.m^{-1}s^{-1}; Young's Modulus $E = 0.6$ GPa; Poisson ratio $\sigma = 0.3$; Restitution coefficient $e = 0.9$ Friction coefficient 0.4; time step for CFD 5×10^{-5} s; time step for DEM 1×10^{-6} s. The corresponding parameters of Young's Modulus, Poisson ratio, restitution coefficient and friction coefficient were considered based on the studies Tsuji *et al.* (1992); Hoomans *et al.* (1996); Zhou *et al.* (2010).

3. Results and Discussion

3.1 Fluidized Bed

In this section, we present the results of the main behavior of gas-solid fluidized beds. Figure 1 presents instantaneous snapshots of the bed with $N = 600$ particles and for the two flow rates, $\overline{U} = 1.05$ and $\overline{U} = 1.15$ m/s, respectively. The corresponding times are: $t = 0$, $t = 1$,$t = 1.5$, $t = 2$,$t = 2.5$, $t = 3$, $t = 3.5$, $t = 4$ and $t = 4.5$ seconds.

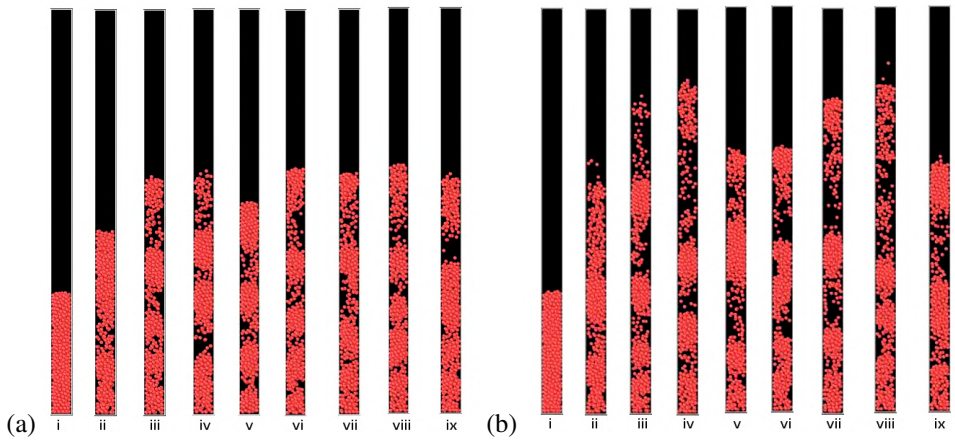

Figure 1. $N = 600$, $\overline{U} = 1.05$ m/s and $\overline{U} = 1.15$ m/s, times i) $t = 0$ s; ii) $t = 1$ s; iii) $t = 1.5$ s; iv) $t = 2$ s; v) $t = 2.5$ s; vi) $t = 3$ s; vii) $t = 3.5$ s; viii) $t = 4$ s; ix) $t = 4.5$ s.

In the simulated conditions, granular plugs and bubbles occupying the entire tube cross section were observed in the fluidized bed. These patterns presented almost one-dimensional shape, that propagates upwards and downwards with characteristic lengths and velocities. The curve in Fig. 2 represents the solid volume fraction (SVF) of the granular bed inside the tube. Regions of high-compactness of particles, where SVF is greater than 0.5, were considered as plugs. Thus, based on the SVF curve, we have identified and followed the particles in each granular plug and bubble over the 5 seconds of simulation.

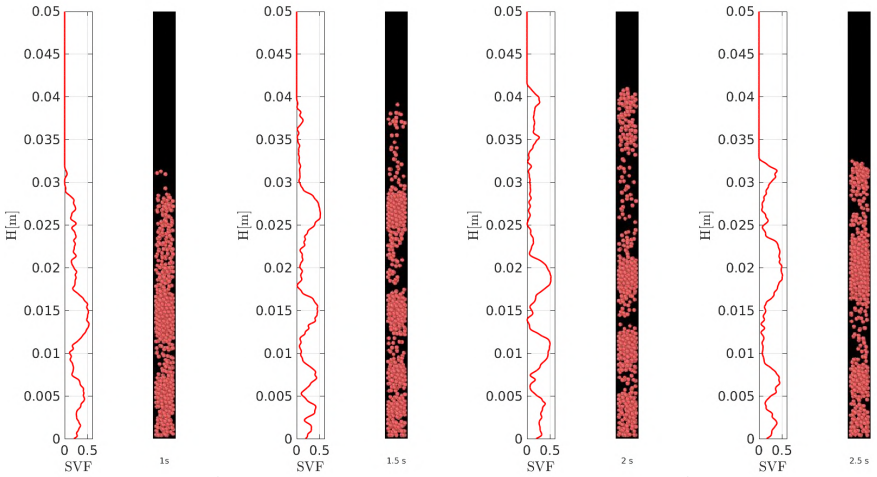

(a) (b) (c) (d)

Figure 2. SVF curve, $N = 600$ and $\overline{U} = 1.15$ m/s, times a) $t = 1$ s; b) $t = 1.5$ s; c) $t = 2$ s; d) $t = 2.5$ s.

3.2 Granular Temperature

The definition of granular temperature arises from an analogy between the fluctuating motion of individual particles in granular systems and the thermal motion of molecules in kinetic theory. The concept of granular temperature has been shown to be extremely effective in characterizing the flow behavior in fluidized beds, as well as in general granular flows (Campbell, 2006). The existence of an anisotropy at the granular temperature indicates that the motion of the particles is directly responsible for the momentum transfer, i.e., the particles move in relation to the local average velocity and, thus, transport their momentum through the system. On the other hand, from momentum transfers due to collisions between particles, an isotropic granular temperature appears (Holland *et al.*, 2008; Jung *et al.*, 2005; Tang *et al.*, 2016; Tartan and Gidaspow, 2004). This anisotropy at the granular temperature was predicted by the Koch and Sangani (1999) studies, these authors showed that the production of the granular temperature is due to shear while its dissipation is due to fluid-particle drag and/or inelastic collisions.

The fluctuating velocities of the particles are the main point to define the granular temperature in a particulate system. For systems that evolve in time, an apparent granular temperature might be defined based on the fluctuations in the bulk motion as a function of time (Jung *et al.*, 2005). In addition, a granular temperature can be defined based on the velocities fluctuations due to the interaction between the solid phase and the gas phase (Campbell, 2006). In general, in all previous works, these definitions of granular temperature are reasonable, the important point to define the granular temperature of a particle system being to establish the objective of the investigation to be done. For instance, in the kinetic theory of granular flows, it is interesting to understand the relative (translational) motion between particles, in this sense, we consider in this study the definition of granular temperature characterizing these particle fluctuation velocities which is given as follows. The velocity fluctuation is given by the measured instantaneous particle velocity $v(\vec{x}, t)$ minus the mean velocity of particles $\langle v(\vec{x}, t)\rangle$. The mean velocity of is defined as

$$\langle v_k(t)\rangle = \frac{1}{n}\sum_{i=1}^{n} v_k(i,t) \tag{9}$$

where k represents x, y, and z directions and n is the number of particles in unit volume applied for spatial averaging. The granular temperature is defined as

$$\theta(t) = \frac{\theta_x + \theta_y + \theta_z}{3} \tag{10}$$

where

$$\theta_k(t) = \frac{1}{n}\sum_{i=1}^{n}\left[v_k(i,t) - \langle v_k(t)\rangle\right]^2. \tag{11}$$

Note that the granular temperatures in this work correspond to the particle granular temperature reported by Jung *et al.* (2005).

Consider the square mean of the velocity fluctuations of each particle as a function of time t is given by:

$$T(t) = \frac{T_x(t) + T_y(t) + T_z(t)}{3} \tag{12}$$

where $T_k(t) = [v_k(t) - \langle v_k(t) \rangle]^2$ with $k = x, y, z$. Figure 3 presents the positions of the center of the particles in the x, z directions and the color bar represents the intensity of $T(t)$, in the corresponding times $t = 1$, $t = 2$,$t = 2.5$, $t = 3$, $t = 3.5$ and $t = 4$ seconds. Note that, in the Fig. 3, there are regions that show homogeneous fluctuations. In regions

(a)

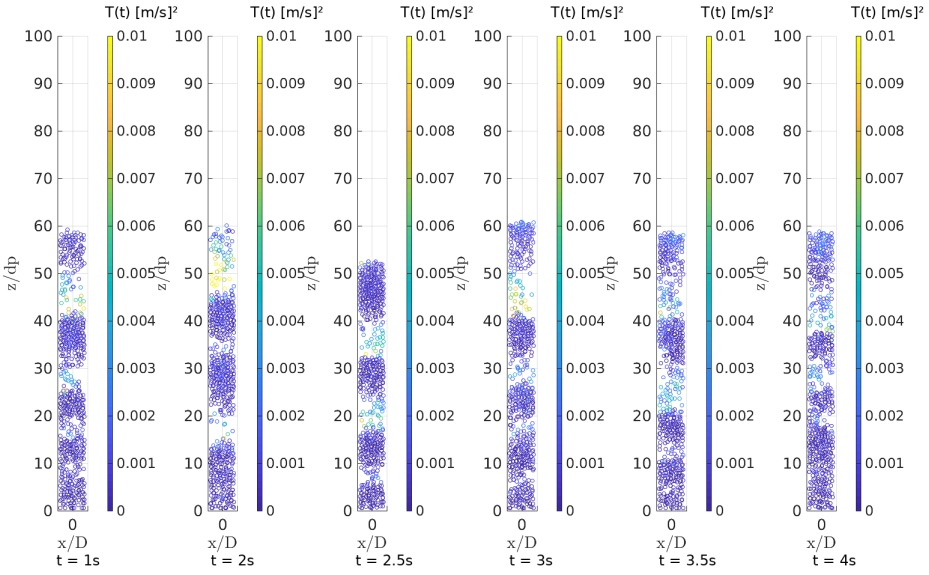

(b)

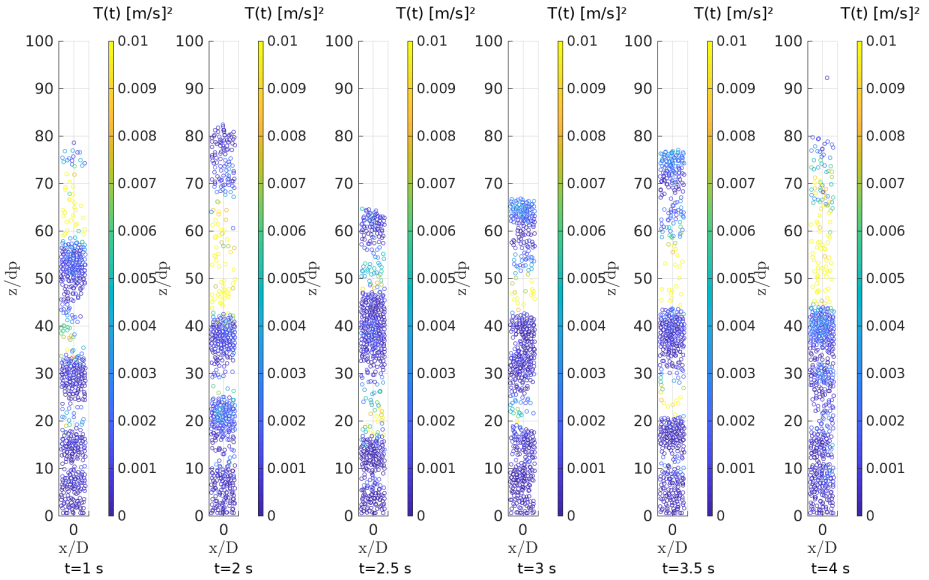

Figure 3. $N = 600$. a) $\overline{U} = 1.05$ m/s; b) $\overline{U} = 1.15$ m/s

of high particle compactness, where SVF is close to 0.5, the square mean of the particles velocities fluctuations is low, and where there is low compactness is high. Plugs have low oscillation of particles, and bubbles high oscillation. As the granular temperature is a property calculated as a local average due to the oscillation of particles in small regions, to avoid statistical errors, we've chosen these regions of plugs and bubbles where the fluctuations are homogeneous to calculate the granular temperature.

From Eqs. 10 and 11, we calculated θ_P in the plug and θ_B in the bubble. Figure 4 shows the granular temperatures, θ_P and θ_B during 4 seconds of simulation.

The granular temperatures oscillate along time. θ_B has larger values because of the instensity of the particle oscilations is much higher at bubble formation in a nonhomogeneous bubbling bed. The values in the flow direction are an order of magnitude larger than those for the x, y direction in a bubble-flow regime. This can be attributed to the dominating

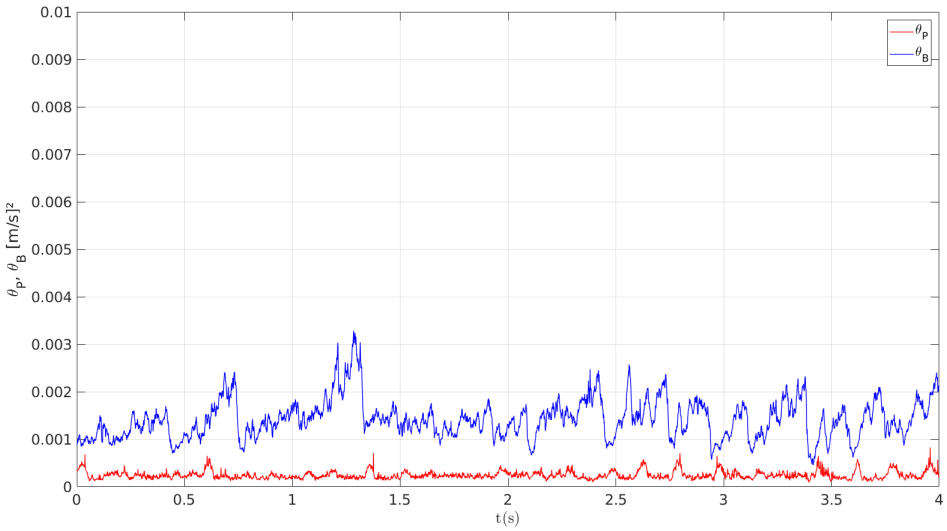

(a)

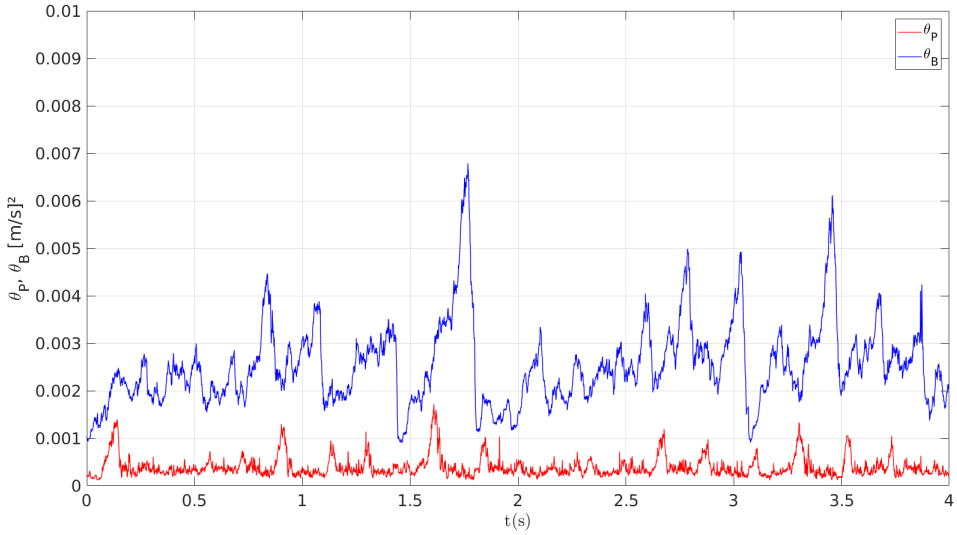

(b)

Figure 4. Granular Temperature θ_P and θ_B. $N = 600$. a) $\overline{U} = 1.05$ m/s; b) $\overline{U} = 1.15$ m/s

influence by the motion of bubbles on the motion of particles on the macroscopic granular temperature. The highest peaks in the graph of the granular temperature θ_P are related to the velocity that the plug reaches at the top of the bed. This observation implies that the highest values of the granular temperature θ_P appear when the topmost plug velocity is reached, since grains are more free to oscillate in that position.

There is an anisotropic behavior of the granular temperature, θ_P and θ_B, revealed in the Figs. 5 and 6. Both granular temperatures in the direction of the flow are much more pronounced than in the transversal directions. The ratios of $\frac{\theta_{Pz}}{\theta_{Px}}$, $\frac{\theta_{Pz}}{\theta_{Py}}$ and $\frac{\theta_{Bz}}{\theta_{Bx}}$, $\frac{\theta_{Bz}}{\theta_{By}}$ are on average 4.06, 4.1 and 14.7, 14.9, respectively. The anisotropy obtained from our simulations is in agreement with the reported observations for the granular temperature by Holland *et al.* (2008); Müller *et al.* (2008); Tartan and Gidaspow (2004).

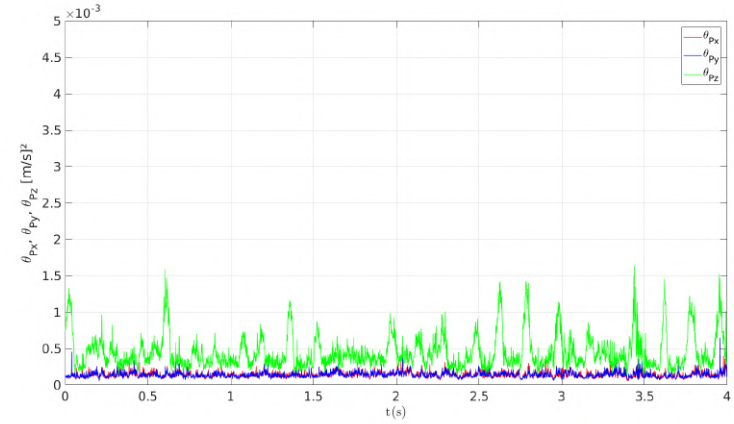

(a)

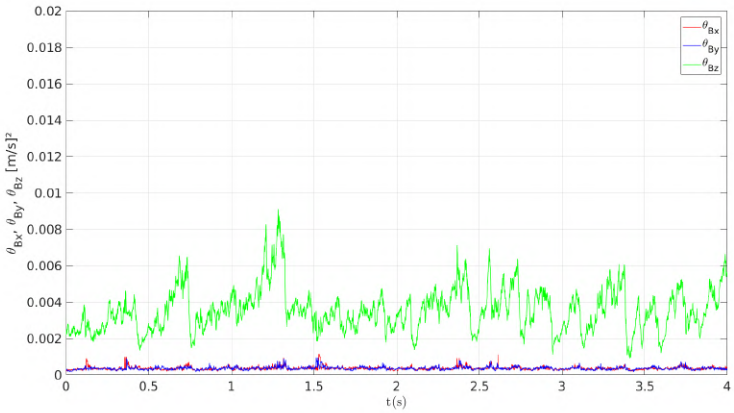

(b)

Figure 5. $N = 600$. $\overline{U} = 1.05$ m/s. Granular Temperature Components a) θ_{Px}, θ_{Py}, θ_{Pz}; b) θ_{Bx}, θ_{By}, θ_{Bz}.

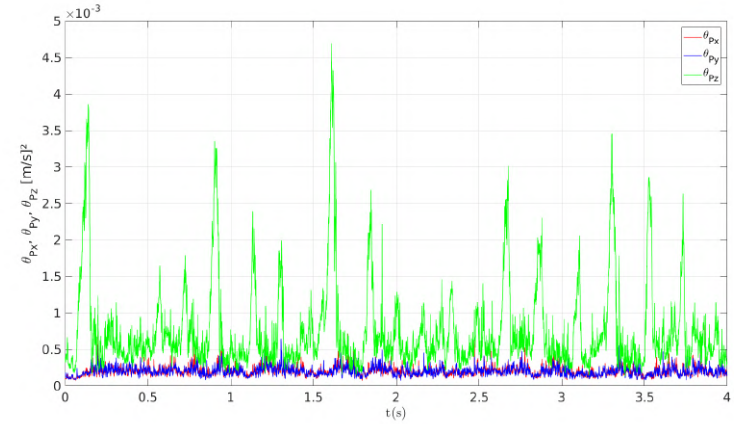

(a)

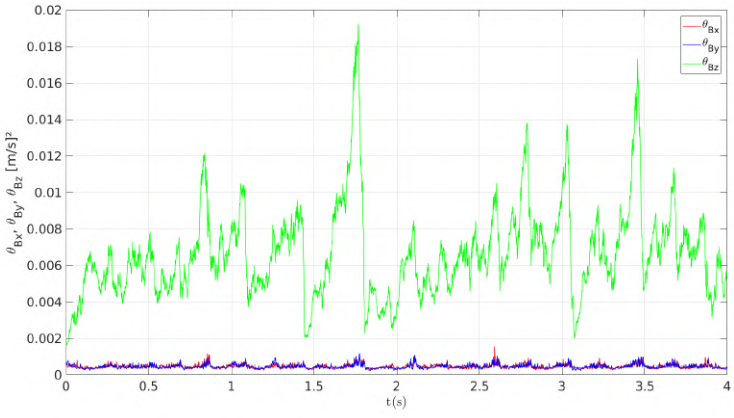

(b)

Figure 6. $N = 600$. $\overline{U} = 1.15$ m/s. Granular Temperature Components a) θ_{Px}, θ_{Py}, θ_{Pz}; b) θ_{Bx}, θ_{By}, θ_{Bz}.

4. CONCLUSIONS

This work investigated numerically the granular temperature in a gas-solid fluidized bed. The granular temperature was computed by averaging the instantaneous velocities by using the concepts of kinetic theory. We observed the formation of alternating high- and low-compactness regions, known as plugs and bubbles, and we tracked every single particle and the local volume fraction to obtain the main behavior of the granular temperature in plugs and bubbles.

The numerical simulations were based on the Eulerian-Lagrangian method. We performed three dimensional simulations using a CFD-DEM method with the open source code CFDEM. The bed was arranged consisting of 600 glass beads, and two air flows that corresponded to cross-sectional mean velocities of $\overline{U} = 1.05$ and $\overline{U} = 1.15$ m/s were imposed. Based on the SVF curve, we have identified and followed the particles in each granular plugs and bubbles in simulations using numerical scripts written in MATLAB.

A difference in the magnitudes of the granular temperature was observed. The values for the flow direction, (z direction), are one order of magnitude larger than those for the transverse directions, (x, y direction). These high values are due to the higher particle oscillations in the flow direction. We found an anisotropy that appears in the flow direction, which is consistent with other studies reported in literature.

5. ACKNOWLEDGEMENTS

Fernando Cúñez is grateful to FAPESP (Grants no. 2016/18189-0 and 2018/23838-3) and Erick Franklin to FAPESP (Grant No. 2018/14981-7), and to CNPq (Grant No. 400284/2016-2) for the financial support provided. Karlo Rocha is grateful to the IFES-FEM/UNICAMP Dinter.

6. REFERENCES

Cammarata, L., Lettieri, P., Micale, G. and Colman, D., 2003. "2d and 3d cfd simulations of bubbling fluidized beds using eulerian-eulerian models". *International J. of Chemical Reactor Engineering*.

Campbell, C.S., 2006. "Granular material flows - an overview." *Powder Technol.*, Vol. 162, pp. 208–229.

Cúñez, F.D. and Franklin, E.M., 2019. "Plug regime in water fluidized beds in very narrow tubes". *Powder Technol.*, Vol. 345, pp. 234–246.

Cúñez, F.D. and Franklin, E.M., 2020a. "Crystallization and jamming in narrow fluidized beds". *Physics of Fluids*, Vol. 32, p. 083303.

Cúñez, F.D. and Franklin, E.M., 2020b. "Mimicking layer inversion in solid-liquid fluidized beds in narrow tubes". *Powder Technol.*, Vol. 364, pp. 994–1008.

Cundall, P.A. and Strack, O.D., 1979. "A discrete numerical model for granular assemblies". *Géotechnique*, Vol. 29, No. 1, pp. 47–65.

Gidaspow, D., 1994. *Multiphase flow and fluidization: continuum and kinetic theory descriptions*. Academic press.

Goldschmidt, M.V., Beetstra, R. and Kuipers, J.M., 2002. "Hydrodynamic modelling of dense gas-fluidised beds: Comparison of the kinetic theory of granular flow with 3d hard-sphere discrete particle simulations". *Chemical Engineerin Science*, Vol. 57, pp. 2059–2075.

Holland, D.J., MÃijller, C.R., Dennis, J.S., Gladden, L.F. and Sederman, A.J., 2008. "Spatially resolved measurement of anisotropic granular temperature in gas-fluidized beds." *Powder Technol.*, Vol. 182, pp. 171–181.

Hoomans, P.B., Kuipers, M., A., Brierls, W.J. and Van Swaaij, P.M., 1996. "Discrete particle simulation of bubble and slug formation in a two dimensional gas-fluidised bed: a hard-sphere approach". *Chemical Engineerin Science*, Vol. 51, No. 1, pp. 99–118.

Hosseini, S.H., Rahimi, R., Zivdar, M. and Samimi, A., 2009. "Cfd simulation of gas-solid bubbling fluidized bed containing fcc particles." *Korean J. Chem. Eng.*, Vol. 26(5), pp. 1405–1413.

Jung, J., Gidaspow, D. and Gamwo, I.K., 2005. "Measurement of two kinds of granular temperatures, stresses, and dispersion in bubbling beds." *Industrial and Engineering Chemistry Research.*, Vol. 44, pp. 1329–1341.

Kafui, K.D., Thornton, C. and Adams, M.J., 2002. "Discrete particle-continuum fluid modelling of gas-solid fuidised beds". *Chemical Engineerin Science*, Vol. 57, pp. 2395–2410.

Koch, D.L. and Sangani, A.S., 1999. "Particle pressure and marginal stability limits for a homogeneous monodisperse gas-fluidized bed: Kinetic theory and numerical simulations." *J. Fluid Mech.*, Vol. 400, pp. 229–263.

Mahinpey, N., Vejahati, F. and Ellis, N., 2007. "Cfd simulation of gas-solid bubbling fluidized bed: an extensive assessment of drag models." *WIT Transactions on Engineering Sciences*, Vol. 56, pp. 51–60.

Müller, C.R., Holland, D.J., Sederman, A.J., Scott, S.A., Dennis, J.S. and Gladden, L.F., 2008. "Granular temperature: Comparison of magnetic resonance measurements with discrete element model simulations." *Powder Technol.*, Vol. 184, pp. 241–253.

Tang, Y., Lau, Y.M., Deen, N.G., Peters, E.A. and Kuipers, J.A., 2016. "Direct numerical simulations and experiments of a pseudo-2d gas-fluidized bed." *Chemical Engineering Science.*, Vol. 143, pp. 166–180.

Tartan, M. and Gidaspow, D., 2004. "Measurement of granular temperature and stresses in risers." *AIChE Journal.*, Vol. 50, pp. 1760–1775.

Tsuji, Y., Tanaka, T. and Ishida, T., 1992. "Lagrangian numerical simulation of plug flow of cohesionless particles in a horizontal pipe". *Powder Technol.*, Vol. 71, No. 3, pp. 239–250.

Wu, G., Ouyang, J. and Li, Q., 2013. "Revised drag calculation method for coarse grid lagrangian-eulerian simulation of gasâĂŞsolid bubblingfluidized bed". *Powder Technol.*, Vol. 235, pp. 959–967.

Xu, M., Ge, W. and Li, J., 2007. "A discrete particle model for particle-fluid flow with considerations of sub-grid structures". *Chemical Engineerin Science*, Vol. 62, pp. 2302–2308.

Zhou, Z.Y., Kuang, S.B., Chu, K.W. and Yu, A.B., 2010. "Discrete particle simulation of particle fluid flow: model formulations and their applicability". *J. Fluid Mech.*, Vol. 661, pp. 482–510.